Supplementary Information

Materials

Analytical grade vanadium Pentoxide (V_2O_5), was purchased from US Research Nanomaterials Inc. Laboratory grade Ethanol was purchased from Sigma-Aldrich. The UV curable epoxy resin was type NOA-81, Norland Products.

Sample Mounting for PIC-PXCT

To ensure a homogenous dispersion of crystalline material for PIC image acquisition, 1 mg of the purchased V_2O_5 powder was dispersed in 10 ml of EtOH and sonicated 2 times for 15 minutes each. Following, 5 µl of this slurry was deposited on a silicon nitride membrane, 1.5 mm in diameter -1000 nm thick, and left to dry in air. The silicon nitride membrane was as a result populated by apparently individual V_2O_5 crystals and polycrystalline aggregates ranging from 200 nm to 20 µm in diameter. The membrane was then mounted on a 2-pin sample holder, constructed of OMNY pins.[1] See Supplementary Figure S1 for details.

Optical and Electron Microscopy

Scanning electron microscopy (SEM) of the samples was carried out using an FEI Nova NanoSEM 650. Optical Micrographs were acquired using a Leica DM2500M. See Supplementary Figures S3 and S4.

PIC-Ptychography

X-ray ptychography is a lensless imaging technique in which the phase problem is solved by means of iterative phase retrieval algorithms and as such provides the complex-valued refractive index of the specimen imaged, i.e. images of both absorption and phase contrast are obtained.[2, 3]

Data Acquisition, Ptychographic Reconstruction and Spatial Resolution Estimation at a Single Energy: PIC-PXCT experiments were carried out at the cSAXS beamline of the Swiss light source (SLS). The photon energy was selected using a double-crystal Si(111) monochromator. Measurements were carried out around the vanadium *K*-edge, 5.460 to 5.520 keV. A Fresnel zone plate with 120 µm diameter, outermost zone width of 60 nm, and locally displaced zones to provide perturbations of the illumination wavefront, was used to define the illumination onto the sample.[4] As the focal length of the zone plate changes with beam energy, the sample to zone plate distance was adjusted so that the focused beam had a diameter of ~5 µm at the sample plane for all energies. Based on this illumination diameter we then set a constant scanning step size for all projections of 0.6 µm using a Fermat spiral scanning grid[5] therewith ensuring sufficient overlap at all energies. Coherent diffraction patterns were acquired with an in-vacuum 1.5k Eiger detector with a 75 µm pixel size approximately 7.2 m downstream of the sample.[6, 7] An evacuated flight tube was positioned between the sample and detector to reduce air scattering and absorption. Measurements were carried out using the positioning instrumentation described in Holler *et al*.[8, 9] at room temperature.

Ptychographic scans consisting of 624 diffraction patterns at maximum were acquired each with an exposure time of 0.1 seconds. From each diffraction pattern a region of 440 × 440 pixels was used in the ptychographic reconstructions. Reconstructions were obtained with 1000 iterations of the difference-map algorithm[2] followed by 500 iterations of maximum likelihood refinement[10, 11] using the PtychoShelves package.[12]

The spatial resolution of a ptychographic image reconstruction was estimated by Fourier ring correlation (FRC).[13] Two independently acquired ptychographic images of the same area, taken at a photon energy below the V *K*-edge were used for this purpose. The estimation is based on the intersection of FRC curves with a one-bit threshold curve.[13] Please see Supplementary Figure S2 for the corresponding correlation curves.

Although the complex-valued transmissivity is reconstructed with both phase and amplitude/ absorption components simultaneously, phase image reconstructions, in the studied X-ray energy range and for the given sample, possess a higher spatial resolution compared to the absorption reconstructions. This is because the real

part of the refractive index decrement is on average 10 times larger than the imaginary part across the studied X-ray energy range, as such phase contrast provides a better signal-to-noise ratio and in turn image reconstructions of higher spatial resolution. This situation is further evident in the spatial resolution of the complex-valued image reconstruction tending strongly towards the phase estimate.

The X-ray dose imparted to the sample per ptychographic scan was estimated to be ~10^6 Gy. The dose was estimated based on the accumulated area flux density during a scan and the mass density of the specimen.[14]

Acquisition and Reconstruction of PIC-Ptychography Datasets: The image acquisition and reconstruction procedure outlined above was carried out 2 times, at 0 and 90 degrees of sample rotation normal to the fixed linear beam polarisation and repeated at ~60 energies across the vanadium *K*-edge. The pre-edge and edge region was scanned in 0.5 eV steps. Since the pixel size depends on the photon energy the reconstructed projections were resized to the largest pixel size. A region of the field of view without particle was used to estimate and remove the constant and linear phase components, perform phase unwrapping, and to normalize the transmission/absorption.[15] Lastly projections were aligned with subpixel accuracy[16] resulting in a complex-valued X-ray transmission near-edge spectrum (XTNES) image stack per polarisation state, i.e. stacks of phase and absorption as a function of energy.

In total, we collected a PIC-Ptychography dataset for each of three different sets of polycrystalline particles located on the same silicon nitride membrane, one of which is shown and discussed in the main text. All datasets show similar results.

Micro-spectroscopy Analysis: Following reconstruction, the two hyperspectral and complex-valued image stacks, measured with orthogonal linear polarization, were first rotated to a common orientation and then spatially registered by means of a normalized mutual information metric.[17] Pixel-level absorption and phase spectra were next normalized to account for variations in sample thickness, i.e. to retrieve numerically comparable pre-edge intensities across both polarisation states. Considering that the sample is entirely consistent of V_2O_5, said normalisation was performed based on the magnitude of the absorption edge jump, or magnitude of the phase drop, respectively, as these quantities are proportional to the total vanadium concentration and thereby proportional to the local sample thickness. The pixel-level X-ray absorption near edge spectra (XANES) and X-ray phase near edge spectra (XPNES) were further normalized through linear regression of pre- and post-edge regions.

Rudimentary crystal grain visualisation, Figure 3, was achieved by mapping to cyan and magenta the pre-edge intensities from 0 and 90 degrees polarisation angle, respectively.

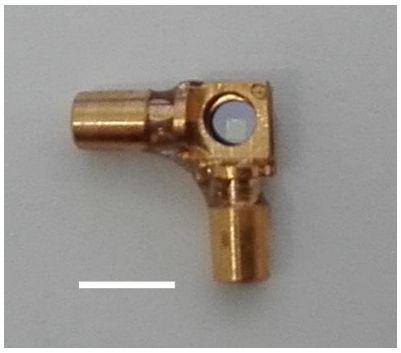

Figure S1. Optical Micrograph of the 2-Pin Sample Holder. To facilitate the acquisition of images at two sample-relative polarization states, we constructed a simple 2-pin sample holder, as shown above. The holder was created by fixing two OMNY sample holder pins (Membrane Type) at ~90 degrees to each other. The silicon nitride membrane, carrying the sample, was then glued onto this holder. Scale bar is 5 mm. Measurements were carried out with a fixed horizontal beam polarisation, following the acquisition of the first spectral image series the sample holder was azimuthally rotated to create the second polarization state with respect to the sample.

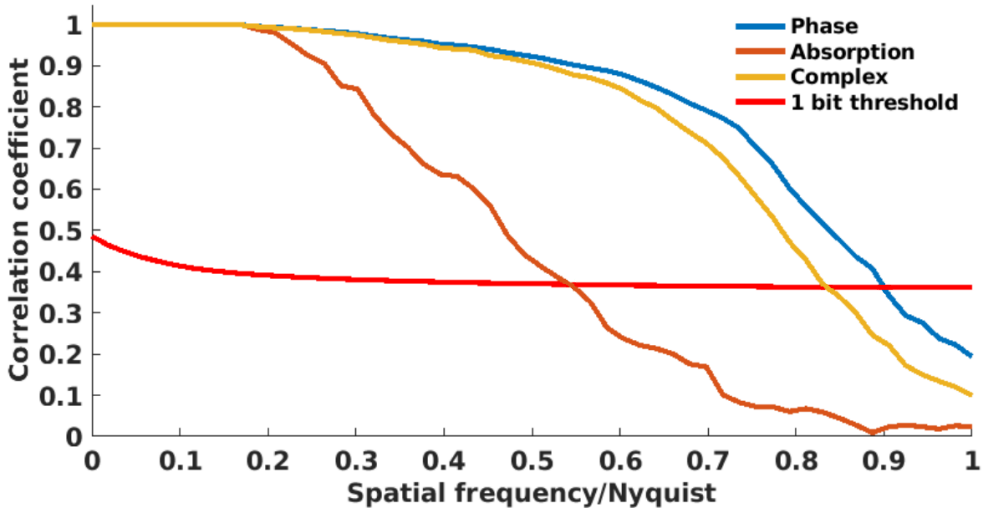

Figure S2. Spatial Resolution of Ptychographic Image Reconstructions. Fourier ring correlation (FRC) curves were calculated from ptychographic images acquired below the V *K*-edge at a single polarisation state. The resolution estimate is based on the one-bit threshold criterion. Pixel size is (48.82 nm).

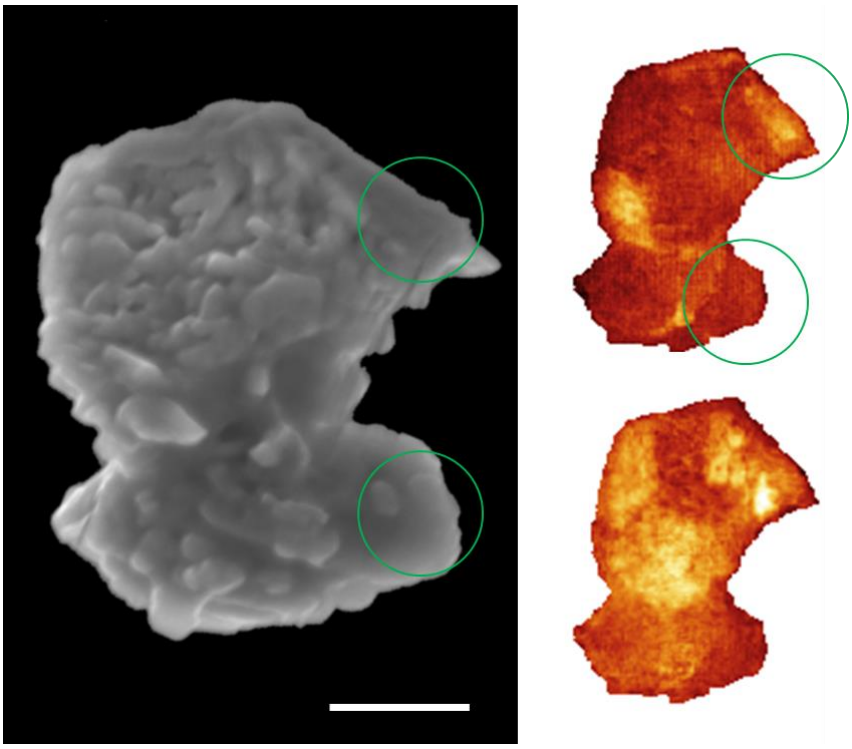

Figure S3. Comparison of Scanning Electron Micrograph and PIC-Ptychography Pre-Peak Intensity Maps of one of the Investigated Vanadium Pentoxide Particles. Left, scanning electron micrograph. Scale bar 2 µm. Right, phase-based pre-peak intensity maps at orthogonal linear polarisation states as shown in Figure 2. φ =0 (top) to φ =90º (bottom). Green circles indicate two dominant crystal grains (CGs) visible in both the surface-sensitive electron microscopy and the transmission based PIC-Ptychography.

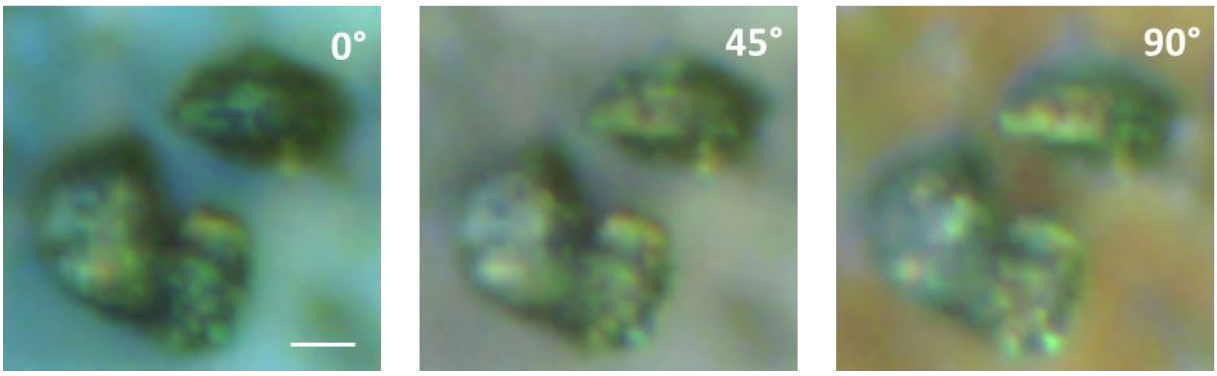

Figure S4. Vanadium Pentoxide Crystals under a Polarizing Optical Microscope. Optical micrographs of the vanadium pentoxide particles shown in the main text acquired at increasingly crossed polarizers, i.e. 0, 45 and 90 degrees. Scale bar is 2 µm.

Supplementary Movie S1. Ptychographic Phase and Absorption Image Reconstructions across the Vanadium *K*-edge. Shown is an excerpt of the acquired the spectral-image series used in the main text, highlighted is the transition from pre-edge to white line. To note is the feature/contrast delay from phase to absorption in accordance with the spectra presented in Figure 1.

Supplementary References:

1. M. Holler, J. Raabe, R. Wepf, S. H. Shahmoradian, A. Diaz, B. Sarafimov, T. Lachat, H. Walther and M. Vitins, *Review of Scientific Instruments*, 2017, **88**, 113701.
2. P. Thibault, M. Dierolf, A. Menzel, O. Bunk, C. David and F. Pfeiffer, *Science*, 2008, **321**, 379-382.
3. F. Pfeiffer, *Nature Photonics*, 2018, **12**, 9-17.
4. M. Odstrčil, M. Lebugle, M. Guizar-Sicairos, C. David and M. Holler, *Optics Express*, 2019, **27**, 14981-14997.
5. X. Huang, H. Yan, R. Harder, Y. Hwu, I. K. Robinson and Y. S. Chu, *Optics Express*, 2014, **22**, 12634-12644.
6. I. Johnson, A. Bergamaschi, H. Billich, S. Cartier, R. Dinapoli, D. Greiffenberg, M. Guizar-Sicairos, B. Henrich, J. Jungmann, D. Mezza, A. Mozzanica, B. Schmitt, X. Shi and G. Tinti, *Journal of Instrumentation*, 2014, **9**, C05032.
7. M. Guizar-Sicairos, I. Johnson, A. Diaz, M. Holler, P. Karvinen, H.-C. Stadler, R. Dinapoli, O. Bunk and A. Menzel, *Optics Express*, 2014, **22**, 14859-14870.
8. M. Holler, J. Raabe, A. Diaz, M. Guizar-Sicairos, C. Quitmann, A. Menzel and O. Bunk, *Review of Scientific Instruments*, 2012, **83**, 073703.
9. M. Holler and J. Raabe, *Optical Engineering*, 2015, **54**, 054101-054101.
10. M. Guizar-Sicairos and J. R. Fienup, *Optics Express*, 2008, **16**, 7264-7278.
11. P. Thibault and M. Guizar-Sicairos, *New Journal of Physics*, 2012, **14**, 063004.
12. K. Wakonig, H.-C. Stadler, M. Odstrcil, E. H. R. Tsai, A. Diaz, M. Holler, I. Usov, J. Raabe, A. Menzel and M. Guizar-Sicairos, *Journal of Applied Crystallography*, 2020, **53**.
13. M. van Heel and M. Schatz, *Journal of Structural Biology*, 2005, **151**, 250-262.
14. M. R. Howells, T. Beetz, H. N. Chapman, C. Cui, J. M. Holton, C. J. Jacobsen, J. Kirz, E. Lima, S. Marchesini, H. Miao, D. Sayre, D. A. Shapiro, J. C. H. Spence and D. Starodub, *Journal of Electron Spectroscopy and Related Phenomena*, 2009, **170**, 4-12.
15. M. Guizar-Sicairos, A. Diaz, M. Holler, M. S. Lucas, A. Menzel, R. A. Wepf and O. Bunk, *Optics Express*, 2011, **19**, 21345-21357.
16. M. Guizar-Sicairos, S. T. Thurman and J. R. Fienup, *Optics Letters*, 2008, **33**, 156-158.
17. C. Studholme, D. L. G. Hill and D. J. Hawkes, *Pattern Recognition*, 1999, **32**, 71-86.
18. D. C. Koningsberger and R. Prins, *X-ray absorption: principles, applications, techniques of EXAFS, SEXAFS, and XANES*, John Wiley and Sons, New York, 1988.